Engineering Solid Mechanics 13 (2025) 243-258

Contents lists available at GrowingScience

Engineering Solid Mechanics

homepage: www.GrowingScience.com/esm

Nonlinear support effects on the aeroelastic stability of multi-stage turbine rotors

Masoud Yousefi[a], R. D. Firouz-Abadi[a] and Hassan Haddadpour[a*]

[a]*Department of Aerospace Engineering, Sharif University of Technology, P.O. Box 11155-8639, Tehran, Iran*

A R T I C L E I N F O

Article history:
Received 24 January 2025
Accepted 26 May 2025
Available online
26 May 2025

Keywords:
Turbine rotor
Aerodynamic force
Aeroelastic Stability
Nonlinear support

A B S T R A C T

This study presents a comprehensive analysis of aeroelastic stability in multi-stage turbine rotors mounted on nonlinear supports. A high-fidelity dynamic model is developed by coupling the structural behavior of a rotating shaft–disk–blade assembly with quasi-steady aerodynamic forces. The system incorporates nonlinear stiffness and damping in the bearing supports, and the governing equations of motion are derived using the Lagrangian method. Aerodynamic forces are modeled using cascade theory for incompressible subsonic flow and integrated with structural dynamics through coordinate transformation. The resulting nonlinear system is solved using the Runge-Kutta method, and its stability characteristics are investigated via bifurcation diagrams and Poincaré maps. A detailed parametric study is conducted to examine the influence of aerodynamic parameters, structural parameters and support characteristics on rotor response. Results show that nonlinear supports significantly alter stability boundaries, reduce critical flutter speeds, and introduce multi-periodic dynamic behavior. These findings provide valuable insights into the design and tuning of support systems to enhance the dynamic robustness of turbomachinery.

1. Introduction

Rotating systems are widely used in industries such as aerospace, petrochemical, power generation, and automotive. Due to the increasing demand for these systems in recent decades, research on the stability of rotating machines has become of great importance. Understanding how various parameters affect the system response can prevent catastrophic failures in industrial rotating machinery. Accurate characterization of the dynamic response of turbines, compressors, and rotor assemblies subjected to aerodynamic loading necessitates the development of a comprehensive dynamic model. Such a model is critical for predicting system behavior and delineating the boundaries of aeroelastic stability. One of the principal challenges in the advancement of high-efficiency and lightweight aircraft engines lies in the increased vulnerability of high-performance rotating blades to fatigue-related degradation under sustained operational loads (Directorate, 2000). Since the excessive vibration of the turbomachine blades is the main factor of fatigue, it is necessary to design and implement measures to reduce these vibrations. The high temperature and rotational accelerations are two main factors of increasing vibration.

As mentioned earlier, due to the increasing application of rotating machines such as turbines and compressors in various industries, a careful analysis of their behavior will be an important aid to better understand such systems and improve their performance. Investigation of the dynamic behavior and stability of such systems has always been one of the major concerns of various researchers. Reducing fan blade vibrations is one of the most important factors for increasing the durability and reliability of the fan blade of an aeroderivative engine. It is well established that the incorporation of damping materials into blade–disk assemblies can effectively attenuate vibratory responses. Numerous experimental investigations have focused on the role of viscoelastic materials in suppressing vibrations in composite fan blades. This line of research has been notably pursued by the NASA Research Center in collaboration with the University of California, San Diego (UCSD). In a series of

* Corresponding author.
E-mail addresses: haddadpour@sharif.edu (H. Haddadpour)

ISSN 2291-8752 (Online) - ISSN 2291-8744 (Print)

doi: 10.5267/j.esm.2025.5.002

non-rotating vibration experiments conducted at UCSD in 1995, it was demonstrated that the application of viscoelastic damping layers on composite blades enhanced damping capacity by an order of magnitude compared to identical blades without such materials (Kosmatka et al., 1995). Importantly, this enhancement did not significantly compromise structural stiffness. Further investigations by Kosmatka and Mehmed (1998) examined the mechanical performance of composite plates embedded with viscoelastic layers under sustained centrifugal loading, confirming the structural viability of such configurations. Among the various parameters influencing the dynamic behavior of turbine rotors, aerodynamic flow interactions are particularly critical. Moore et al. (2011) quantified destabilizing aerodynamic forces in a centrifugal compressor using a combination of physically modified models and computational fluid dynamics simulations.

Meanwhile, the history and development process of aerodynamics of turbomachinery are of great importance. Several analytical and numerical aerodynamic models have been used to calculate the aerodynamic coefficients of turbomachinery. In the past, semi-analytical models were popular, while nowadays, due to the rapid development of computational speed, numerical models are mainly used. Therefore, the following theories have been introduced for the analytical modeling of the aerodynamic effects on the blades of a single-stage compressor or turbine (Dowell & Dowell, 2015):

1- Whitehead: For subsonic incompressible flow
2- Smith: For subsonic compressible flow
3- Verden: For supersonic compressible flow
4- Adamzyk: For supersonic compressible flow

The methods for modeling the aerodynamic forces are not completely analytical and need to be numerically integrated for finite vortex (the vortex created on the airfoil) along the airfoil chord. For this purpose, the kernel function proposed by Whitehead for incompressible flows in 1964 (Whitehead, 1962) is used. In this hypothesis, the airfoil shape is modeled as a flat plate, and both steady and unsteady flows are modeled in the form of a small deviation from uniform free flow. Whitehead's aerodynamic model was valid for subsonic incompressible flow. Later, in 1972, Smith (Smith, 1972) proposed the aerodynamic theory for subsonic compressible flows. His analysis was based on the solution of the wave, continuity and momentum equations due to the propagation of the vortices and pressure perturbations. Thus, Smith's approach covered the weakness of Whitehead's study in the analysis of compressible flows.

In a similar effort to analyze the internal flow of turbomachinery, Adamzyk (Adamczyk & Goldstein, 1978) studied the supersonic compressible flow in turbomachinery in 1978. In order to predict blade flutter, he placed the low amplitude vibrating blades in an unsteady flow, where, due to the extremely small thickness of the blades, the assumption of a small deviation of the steady flow from the uniform flow was rational. Thus, he described both steady and unsteady flows considering a small perturbation to the main uniform flow. Also, since the unsteady flow was the subject of concern in this study, and due to the importance of blade thickness and camber in perturbations of the steady flow, the blade geometry can be assumed as a flat plate. Furthermore, the fluid was assumed to be an ideal viscous gas with constant specific heat and non-rotational isentropic flow.

After the introduction of aerodynamic theories in the field of turbomachinery, researchers tended to focus on aeroelastic analyses. Recently, in 2017, Seeley et al (2017) managed to perform an experiment to observe the flutter phenomenon and calculate the aerodynamic damping in a turbine blade. They showed that the aerodynamic damping increases from Mach 0.1 to 0.65 and, after a sudden drop, remains constant from Mach 0.8 to 1.2. In 2020, Bornassi et al (Bornassi et al., 2020) also studied the instability speed of a blade in subsonic flow. They applied Smith's theory for flow modeling and showed that the torsional stiffness of a blade has a significant effect on the instability speed variation of that blade. The important point in this research was that the torsional mode was introduced as an active aeroelastic mode.

In addition to aerodynamic effects, bearings and seals play a crucial role in determining the dynamic behavior of rotating machinery (Kim et al., 2014; Li et al., 2022; Liu et al., 2018; Palanca et al., 2020; Żywica et al., 2018). Several studies have focused on the characteristics of gas turbine seals. For example, Subramanian et al. (Subramanian et al., 2016) analyzed the influence of centrifugal growth on the rotor dynamic behavior of a representative rotating labyrinth seal. In a related context, Wang et al. (Wang et al., 2020) employed a free fluid–structure interaction approach to capture the nonlinear dynamic characteristics of plain gas journal bearings with high accuracy. The influence of aerodynamic forces on rotor dynamics has also been extensively investigated. However, unlike previous studies, the present work integrates a comprehensive dynamic model of a turbine rotor with nonlinear bearing supports. While prior research has considered the aerodynamic loading separately, the combined effect of aerodynamic forces and nonlinear support characteristics has received limited attention in the literature. In this study, the governing equations of motion are formulated via Lagrange’s method, and the numerical solution is obtained using the Runge–Kutta integration scheme. This investigation provides a detailed assessment of the key parameters influencing the dynamic response of turbine rotor systems and underscores the significance of both aerodynamic and support-related nonlinearities

2. Formulation

To investigate the influence of flow dynamics on rotor stability, the coupled effects of both translational and rotational motions of the rotor—modeled with four degrees of freedom—are taken into account. Variations in the blade root position induce corresponding alterations in the surrounding flow field, which, in turn, modify the aerodynamic forces and moments acting on the blades. In the following analysis, a dynamic model is formulated for a generalized rotor system composed of multiple disks mounted along a shaft, with each disk supporting a set of blades. This framework enables the assessment of aeroelastic stability for turbines comprising an arbitrary number of blade-disk cascades.

2.1 Rotor Dynamics

According to Fig 3, it is assumed that the translational and rotational movement of the shaft are transmitted to the disk through the mounting location. Therefore, changes in the disk displacement will be a function of the shaft's degrees of freedom. This means that the O-XYZ inertial coordinate system is placed at the center of the shaft. Since the displacements of the center of the disk and its mounting point on the shaft are equal, the movements of the center of the disk are described by Eq. (1) and Fig. 1.

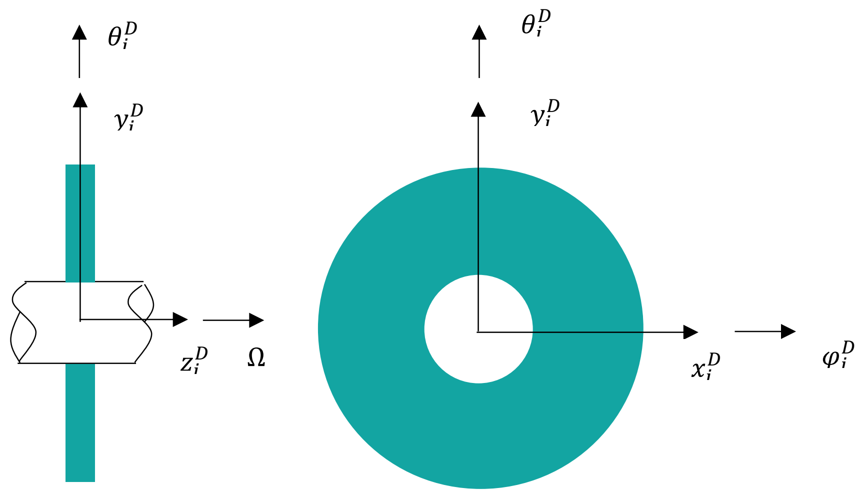

Fig. 1. Disc and blade reference coordinate.

$$q_i^D = \begin{Bmatrix} x_i^D \\ y_i^D \\ \varphi_i^D \\ \theta_i^D \end{Bmatrix} \tag{1}$$

According to the degrees of freedom of the disc in Fig. 3, disc rotates equal to φ about x axis, θ about y axis then, and finally ωt about the new z axis. Assuming that the rotor is balanced, disc rotational speed should be described as the summation of rotational speeds at three directions, which can be written in form of a vector:

$$\Omega = \dot{\varphi} e_{x_0} + \dot{\theta} e_{y_1} + \omega e_{z_2} \tag{2}$$

Using the following transformation matrices, body coordinate system is transferred to the reference coordinate system.

$$R_\varphi = \begin{bmatrix} 1 & 0 & 0 \\ 0 & \cos(\varphi) & -\sin(\varphi) \\ 0 & \sin(\varphi) & \cos(\varphi) \end{bmatrix}$$
$$R_\theta = \begin{bmatrix} \cos(\theta) & 0 & \sin(\theta) \\ 0 & 1 & 0 \\ -\sin(\theta) & 0 & \cos(\theta) \end{bmatrix} \tag{3}$$
$$R_\omega = \begin{bmatrix} \cos(\omega t) & -\sin(\omega t) & 0 \\ -\sin(\omega t) & \cos(\omega t) & 0 \\ 0 & 0 & 1 \end{bmatrix}$$

With the aid of Taylor's expansion and assuming small vibrations, Eq. (3) can be rewritten in the following form:

$$R_\varphi = \begin{bmatrix} 1 & 0 & 0 \\ 0 & 1-\frac{\varphi^2}{2} & -\varphi \\ 0 & \varphi & 1-\frac{\varphi^2}{2} \end{bmatrix}, \qquad R_\theta = \begin{bmatrix} 1-\frac{\theta^2}{2} & 0 & \theta \\ 0 & 1 & 0 \\ -\theta & 0 & 1-\frac{\theta^2}{2} \end{bmatrix} \tag{4}$$

Thus, the rotational speed in the reference coordinate system is resulted as below:

$$\Omega = R_\omega R_\theta \begin{Bmatrix} \dot{\varphi} \\ 0 \\ 0 \end{Bmatrix} + R_\omega \begin{Bmatrix} 0 \\ \dot{\theta} \\ 0 \end{Bmatrix} + \begin{Bmatrix} 0 \\ 0 \\ \omega \end{Bmatrix} \tag{5}$$

Since the rotational speed is calculated in the reference coordinate system and with the assumption of small vibrations and the degrees of freedom considered for the disc (Fig. 1), kinetic energy for a rigid disc can be derived as Eq. (6):

$$T_D = \frac{1}{2}\left(\dot{q}_{D_i}^T \left(M_{D_i}^T + M_{D_i}^R\right)\dot{q}_{D_i} + q_{D_i}^T \Omega g_{D_i}^d \dot{q}_{D_i}\right) \tag{6}$$

$M_{D_i}^T$ and $M_{D_i}^R$ matrices are mass translational and rotational inertia matrices, respectively, defined in form of Eq. (7).

$$M_{D_i}^T = \begin{bmatrix} m_{D_i} & 0 & 0 & 0 \\ 0 & m_{D_i} & 0 & 0 \\ 0 & 0 & 0 & 0 \\ 0 & 0 & 0 & 0 \end{bmatrix}, \qquad M_{D_i}^R = \begin{bmatrix} 0 & 0 & 0 & 0 \\ 0 & 0 & 0 & 0 \\ 0 & 0 & I_{D_i} & 0 \\ 0 & 0 & 0 & I_{D_i} \end{bmatrix} \tag{7}$$

Also, the rigid disc gyroscopic effects matrix, $g_{D_i}^d$, is written as Eq. (8).

$$g_{D_i}^d = \begin{bmatrix} 0 & 0 & 0 & 0 \\ 0 & 0 & 0 & 0 \\ 0 & 0 & 0 & -J_{D_i} \\ 0 & 0 & J_{D_i} & 0 \end{bmatrix} \tag{8}$$

where, m_{D_i}, I_{D_i} and J_{D_i} are disc mass, mass moment of inertia, and polar moment of inertia, respectively. Assuming that the degree of freedom along X axis is equal to U, along Y is equal to V, φ is the rotations about X axis and θ is the rotations about Y axis. The vector representing the degrees of freedom associated with the shaft's center of mass is defined as follows.

$$q_s = \begin{Bmatrix} U \\ V \\ \theta \\ \varphi \end{Bmatrix} \tag{9}$$

Also, the kinetic energy of the shaft with the Jeffcott rotor assumption can be written as:

$$T_r = \frac{1}{2}\bar{V}^T m_r V + \frac{1}{2}\Omega^T J_r \Omega \tag{10}$$

In which *m* is the shaft mass, *V* is the linear velocity vector of the shaft, and J_r, is the shaft moment of inertia defined as:

$$J_r = \begin{bmatrix} J_1 & 0 & 0 \\ 0 & J_2 & 0 \\ 0 & 0 & J_p \end{bmatrix} \tag{11}$$

In order to calculate the rotor linear velocity, we must optain, the position vector of the rotor system. Thus, the position vector of the shaft center of mass in the reference coordinate system is:

$$r = Ue_{x_0} + Ve_{y_0} \tag{12}$$

The velocity vector of the system is written as:

$$\bar{V} = \dot{U}e_{x_0} + \dot{V}e_{y_0} \tag{13}$$

And the kinetic energy of the shaft center of mass is resulted as:

$$\begin{aligned} T_r &= \frac{1}{2}\left(J_{t_1} - J_{t_2}\right)\left(\left(\dot{\varphi}^2 - \dot{\theta}^2\right)\mathbf{cos}^2(\omega t) + \dot{\varphi}\dot{\theta}\,\mathbf{sin}(2\omega t)\right) \\ &+ \frac{1}{2}J_p\left(\dot{\varphi}^2\theta^2 + 2\dot{\varphi}\theta\omega\right) + \frac{1}{2}J_{t_1}\dot{\theta}^2 + \frac{1}{2}J_{t_2}\dot{\varphi}^2 + \frac{1}{2}J_p\omega^2 \\ &+ \frac{1}{2}m\left(\dot{U}^2 + \dot{V}^2\right) \end{aligned} \tag{14}$$

Therefore, the summation of the kinetic energies of the disc, shaft, and blade are in the following form:

$$T = T_r + T_D \tag{15}$$

After calculating the kinetic energy, potential energy of the system needs to be calculated.

$$U_s = \frac{1}{2}\bar{R}^T K_s\, \bar{R} \tag{16}$$

where:

$$\bar{R} = \begin{Bmatrix} U + z\,\theta \\ V - z\,\varphi \end{Bmatrix} \tag{17}$$

and

$$K_s = \begin{bmatrix} K_j & O \\ O & K_i \end{bmatrix}, K_j = \begin{bmatrix} k_{11} & k_{12} \\ k_{12} & k_{22} \end{bmatrix}_j, K_i = \begin{bmatrix} k_{11} & k_{12} \\ k_{12} & k_{22} \end{bmatrix}_i \tag{18}$$

The terms k_{ij} represent the linear stiffness coefficients corresponding to the elastic restoring forces within the system. In addition to linear stiffness, the support nonlinearity is modeled as a symmetric second-order function, characterized by Ku^2 and Kv^2 in the x and y directions, respectively. Assuming the presence of linear viscous damping, the energy dissipation is formulated using Rayleigh's dissipation function. Accordingly, the dissipative effects can be expressed as follows:

$$R_s = \frac{1}{2}\dot{\bar{R}}^T C_s\, \dot{\bar{R}} \tag{19}$$

where:

$$\dot{\bar{R}} = \begin{Bmatrix} \dot{U} + z\,\dot{\theta} \\ \dot{V} - z\,\dot{\varphi} \end{Bmatrix} \tag{20}$$

and

$$C_s = \begin{bmatrix} C_j & O \\ O & C_i \end{bmatrix}, C_j = \begin{bmatrix} c_{11} & c_{12} \\ c_{12} & c_{22} \end{bmatrix}_j, C_i = \begin{bmatrix} c_{11} & c_{12} \\ c_{12} & c_{22} \end{bmatrix}_i \tag{21}$$

which c_{ij} are the damping values of the linear dampers. To derive the system's equations of motion, the Lagrangian method is employed. For a system with four independent generalized coordinates, the corresponding expression takes the following general form:

$$\frac{d}{dt}\frac{\partial L}{\partial \dot{q}_i} - \frac{\partial L}{\partial q_i} = 0 \qquad i = 1,....,4 \tag{22}$$

where:

$$L = T - U \tag{23}$$

Thus, using Eq. (6) and substituting in Eq. (22), the governing dynamic equation of a rotating rigid disc with basic stimulation can be found.

$$\left(M_{D_i}^{T}+M_{D_i}^{R}\right)\ddot{q}_{D_i}+\Omega g_{D_i}^{d}\dot{q}_{D_i}=F_{D_i} \tag{24}$$

Since the effects of the shaft translational and rotational displacements over the disc have been considered, the reaction force and moment at the root is assumed to be acting on the shaft and at the disc attachment location. Considering the governing Jeffcott equation with taking into account the dynamic effects of the discs installed on the shaft, the governing equation of a rotating shaft with n installed discs can be described as Eq. (25).

$$\mathbf{M}\ddot{q}+\Omega\mathbf{G}\dot{q}+\mathbf{C}\dot{q}+\mathbf{K}q=F_N-T_{D_i}^{T}F_{D_i}+T_{D_i}^{T}F_{A_i} \tag{25}$$

In which F_N is the nonlinear force as a result of nonlinear supports, F_{D_i} are the inertial and dynamic effects of the disc and F_{A_i} is the external aerodynamic force applied to the disc. Also, since the aerodynamic force vector and the disc inertial vector are at a distance from the shaft center and each disc is at a different position in main coordinate system, their moments should be considered while moving the forces to the reference point. In order to do so, transition matrix $T_{D_i}^{T}$ is defined as Eq. (26).

$$T_{D_i}^{T}=\begin{bmatrix}1 & 0 & 0 & (L-L_i)\\ 0 & 1 & -(L-L_i) & 0\\ 0 & 0 & 1 & 0\\ 0 & 0 & 0 & 1\end{bmatrix} \tag{26}$$

Also **M**, **G**, **C**, **K**, and F_N are defined as Eq. (27):

$$\mathbf{M}=\begin{bmatrix}m_S & 0 & 0 & 0\\ 0 & m_S & 0 & 0\\ 0 & 0 & I_S & 0\\ 0 & 0 & 0 & I_S\end{bmatrix}\quad \mathbf{G}=\begin{bmatrix}0 & 0 & 0 & 0\\ 0 & 0 & 0 & 0\\ 0 & 0 & 0 & J_p\\ 0 & 0 & -J_p & 0\end{bmatrix}\quad \mathbf{K}=\begin{bmatrix}K_{11} & 0 & 0 & K_{12}\\ 0 & K_{11} & -K_{12} & 0\\ 0 & -K_{12} & K_{22} & 0\\ K_{12} & 0 & 0 & K_{22}\end{bmatrix}$$
$$\mathbf{C}=\begin{bmatrix}C_{11} & 0 & 0 & C_{12}\\ 0 & C_{11} & -C_{12} & 0\\ 0 & -C_{12} & C_{22} & 0\\ C_{12} & 0 & 0 & C_{22}\end{bmatrix}\quad F_N=\begin{bmatrix}f_1\\ f_2\\ f_3\\ f_4\end{bmatrix} \tag{27}$$

In which, m_s, I_s and J_s are shaft mass, mass moment of inertia, and polar moment of inertia, respectively and the components of **C**, **K** and F_N are as below:

$$\begin{aligned}
&K_{11}=k_{x1}+k_{x2},K_{12}=a_1k_{x1}-a_2k_{x2},K_{22}=a_1^2k_{x1}+a_2^2k_{x2}\\
&C_{11}=c_{x1}+c_{x2},C_{12}=a_1c_{x1}-a_2c_{x2},C_{22}=a_1^2c_{x1}+a_2^2c_{x2}\\
&f_1=-2K_{11}^{'}u^3-K_{22}^{'}u\theta^2+3K_{12}^{'}u^2\theta\\
&f_2=-K_{12}^{'}u^3-K_{22}^{'}u^2\theta\\
&f_3=-2K_{11}^{'}v^3-K_{22}^{'}v\phi^2-3K_{12}^{'}v^2\phi\\
&f_4=K_{12}^{'}v^3-K_{22}^{'}v^2\phi\\
&K_{11}^{'}=k_{x1}^{'}+k_{x2}^{'},\ K_{12}^{'}=a_1k_{x1}^{'}-a_2k_{x2}^{'},\ K_{22}^{'}=a_1^2k_{x1}^{'}+a_2^2k_{x2}^{'}
\end{aligned} \tag{28}$$

Thus, inserting Eq. (23) into (24) will result in:

$$\mathbf{M}\ddot{q}+\Omega\mathbf{G}\dot{q}+\mathbf{C}\dot{q}+\mathbf{K}q=F_N-T_{D_i}^{T}\left(M_{D_i}^{T}+M_{D_i}^{R}\right)\ddot{q}_{D_i}-T_{D_i}^{T}\Omega g_{D_i}^{d}\dot{q}_{D_i}+T_{D_i}^{T}F_{A_i} \tag{29}$$

Therefore, the governing dynamic equation of an n-stage turbine can be described as below:

$$\left(\mathbf{M}+\sum_{i=1}^{n}T_{D_i}^{T}\left(M_{D_i}^{T}+M_{D_i}^{R}\right)\right)\ddot{q}+\Omega\left(\mathbf{G}+\sum_{i=1}^{n}T_{D_i}^{T}g_{D_i}^{d}\right)\dot{q}+\mathbf{C}\dot{q}+\mathbf{K}q=F_{N}+\sum_{i=1}^{n}T_{D_i}^{T}F_{A_i} \tag{30}$$

Eq. (30) is the governing dynamic equation of motion of a multistage rotor, which can be generalized to any arbitrary number of stages, with *i* being the disc number on the shaft, and *n* being the total disc count on the shaft.

2.2 Aerodynamics

The disks and blades are assumed to be rigid, so all shaft motion is transferred to the blades at the attachment point. Since the variation at the blade root affects the upstream flow pattern, it reciprocally causes changes in the downwash on the blade and ultimately changes the force applied to the blade. Also, since the blade sections are assumed to be flat plates, the wake at each blade is assumed to be in the form of a straight line from the blade trailing edge. Such changes at the blade root lead to changes in the flow AOA. This change in AOA is directly related to the change in blade speed. Therefore, it is necessary to obtain the velocity field for each blade, and according to the velocity, find the downwash value for each blade. Knowing the downwash, the forces and moments on each blade can be calculated. Forces and moments on the blades are transferred to the disk shaft attachment point and ultimately affect the dynamic parameters and rotor response and dynamic stability. The assumed blade root motions are shown in Eq(31).

$$q_i^b=\begin{Bmatrix}x_i^b\\ y_i^b\\ \varphi_i^b\\ \theta_i^b\end{Bmatrix} \tag{31}$$

It should be noted that according to disc rigidity assumption, the transferred motions to the blades will be assumed to be equal for all the blades attached to the disc.

For calculating the aerodynamic forces and moments, first, the velocity field of each blade should be found. For this aim, the induced flow velocity on the blade caused by shaft movement should be obtained. The induced flow velocity is a result of two translational and rotational movements assumed for the shaft in the following form on the blade:

$$V_b=V_s+\omega_b\times r_b \tag{32}$$

In which, V_s is the blade linear velocity due to translational movements of the shaft and disc, ω_b is the rotational velocity of the blade, and r_b is the position vector of each point on the blad. According to the considered translational movements for the shaft, induced linear velocity of the blade is:

$$V_s=\dot{x}\hat{i}+\dot{y}\hat{j} \tag{33}$$

Also, assuming the blade rotations of φ about the X axis, θ about the Y axis in new coordinate system, and $\psi=\Omega t$ about Z axis in the final coordinate system, angular velocity of each point on the blade is (Fig. 2):

$$\omega_b=\dot{\varphi}e_{x_0}+\dot{\theta}e_{y_1}+\Omega e_{z_2} \tag{34}$$

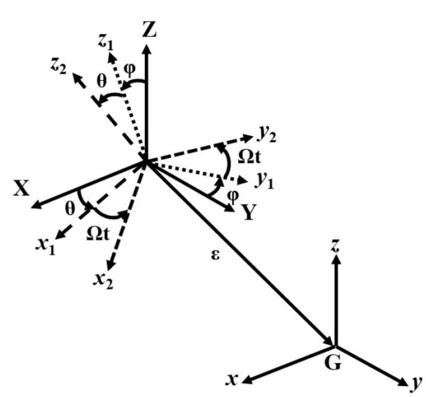

Fig. 2. Coordinate transformation.

Using the transformations of the rotation matrices, induced angular velocity at each point on the blade due to shaft movements in its body coordinates will be equal to:

$$\omega_b = P\hat{i} + Q\hat{j} + R\hat{k} \tag{35}$$

where:

$$\begin{aligned} P &= \dot{\varphi} - \Omega \mathbf{sin}(\theta) \\ Q &= \dot{\theta}\mathbf{cos}(\varphi) + \Omega\mathbf{cos}(\theta)\mathbf{sin}(\varphi) \\ R &= \Omega\mathbf{cos}(\theta)\mathbf{cos}(\varphi) - \dot{\theta}\mathbf{sin}(\varphi) \end{aligned} \tag{36}$$

According to **Fig. 5**, position vector of each blade in inertial coordinate is:

$$r_i = |r|\mathbf{cos}(\beta_j)\hat{i} + |r|\mathbf{sin}(\beta_j)\hat{j} \tag{37}$$

In which $|r|$ is the distance of each point on the blade from the shaft center.

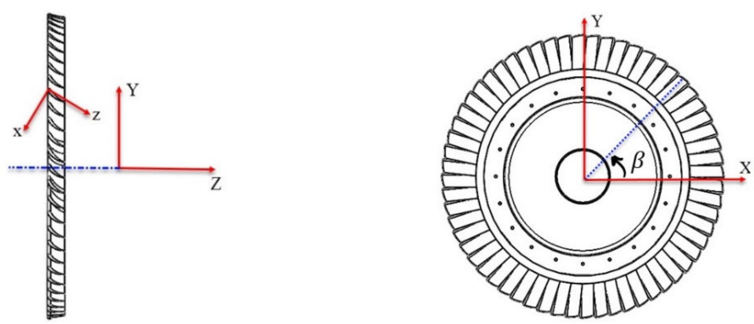

Fig. 3. Blade coordinate system

On the other hand, the upstream flow impacts the blade with a velocity of V_{b_i}. Therefore, the flow velocity on the blade assuming small vibrations is:

$$V_{b_i} = V_x\hat{i} + V_y\hat{j} + V_z\hat{k} \tag{38}$$

where:

$$\begin{aligned} V_x &= \dot{x} - |r|\mathbf{sin}(\beta_i)\left[\Omega\left(1-\frac{1}{2}\theta^2\right)\left(1-\frac{1}{2}\varphi^2\right) - \dot{\theta}\varphi\right] \\ V_y &= \dot{y} + |r|\mathbf{cos}(\beta_i)\left[\Omega\left(1-\frac{1}{2}\theta^2\right)\left(1-\frac{1}{2}\varphi^2\right) - \dot{\theta}\varphi\right] \\ V_z &= -V_\infty + |r|\mathbf{sin}(\beta_i)(\dot{\varphi} - \Omega\theta) - |r|\mathbf{cos}(\beta_i)\left[\left(1-\frac{1}{2}\varphi^2\right)\dot{\theta} + \Omega\left(1-\frac{1}{2}\theta^2\right)\varphi\right] \end{aligned} \tag{39}$$

Thus, downwash is obtained as:

$$\sigma_i = R_i^C \cdot V_{b_i} \tag{40}$$

With R_j^C being the normal vector to the blade chord and is written in the following form:

$$R_i^C = T_\beta T_\alpha T_p r_{b_i}^c \tag{41}$$

And

$$T_\beta = \begin{bmatrix} \mathbf{sin}(\beta_i) & -\mathbf{cos}(\beta_i) & 0 \\ \mathbf{cos}(\beta_i) & \mathbf{sin}(\beta_i) & 0 \\ 0 & 0 & 1 \end{bmatrix}$$
$$T_\alpha = \begin{bmatrix} \mathbf{sin}(\alpha) & 0 & \mathbf{cos}(\alpha) \\ 0 & 1 & 0 \\ -\mathbf{cos}(\alpha) & 0 & \mathbf{sin}(\alpha) \end{bmatrix} \tag{42}$$
$$T_p = \begin{bmatrix} 0 & 0 & 1 \\ 0 & 1 & 0 \\ -1 & 0 & 0 \end{bmatrix}$$

where $r^c_{b_i}$ is the unit vector of the blade chord coordinate system (**Fig. 3**) along the chord. Thus, the applied force on each blade is:

$$F_{b_i} = \rho_\infty V_\infty \Gamma_i \tag{43}$$

In which V_∞ is the upstream flow velocity, ρ_∞ is the upstream flow density, and Γ_i is the total induced rotation of each blade, found from the following relation:

$$\Gamma_i = \int_0^c \sigma_i(x)\,dx \tag{44}$$

Finally, the lift force value and the resulted moment from the induced flow over the cascade with n blades are derived:

$$F_i^D = \sum_{j=1}^{m} F_{b_j}$$
$$M_i^D = \sum_{j=1}^{m}\left(r_j \times F_{b_j}\right) + \sum_{j=1}^{m} \gamma F_j^D \tag{45}$$

It should be added that the relations for aerodynamic forces and moments are obtained at the shaft center. Also, "i" refers to each disc, "j" refers to each blade, and m indicates the total blade number on each disc. Finally:

$$F_{A_i} = \begin{Bmatrix} F_i^D \\ M_i^D \end{Bmatrix} \tag{46}$$

in the other words, the aerodynamic forces and moments values can be defined in terms of the shaft movement parameters as below:

$$F_{A_i} = C_i^a \begin{Bmatrix} \dot{x}_i^D \\ \dot{y}_i^D \\ \dot{\varphi}_i^D \\ \dot{\theta}_i^D \end{Bmatrix} + K_i^a \begin{Bmatrix} x_i^D \\ y_i^D \\ \varphi_i^D \\ \theta_i^D \end{Bmatrix} \tag{47}$$

And thereafter, the coupled aeroelastic equation of the rotor is obtained:

$$\left(\mathbf{M} + \sum_{i=1}^{n} T_{D_i}^{T}\left(M_{D_i}^{T} + M_{D_i}^{R}\right)\right)\ddot{q} + \Omega\left(\mathbf{G} + \sum_{i=1}^{n} T_{D_i}^{T} g_{D_i}^{d}\right)\dot{q} + \left(\mathbf{C} - \sum_{i=1}^{n} T_{D_i}^{T} C_i^{d}\right)\dot{q} + \left(\mathbf{K} - \sum_{i=1}^{n} T_{D_i}^{T} K_i^{d}\right) q = F_N \tag{48}$$

Eq. (48) is the governing dynamic equation of a shaft-disc-blade assembly subject to an aerodynamic flow, which can be generalized to n discs with m blades installed on each disc. This equation will be used later to calculate the aeroelastic stability range of the rotor.

3. Results and Discussion

In this Section, first the proposed formulation is validated and thereafter, system behavior based on the effective parameters is studied.

3.1 Validation

To validate the proposed methodology, a rotory system equipped with linear supports is analyzed for comparison purposes. The results presented in Fig. 4 are benchmarked against those reported in ref (Genta, 2005), demonstrating a high level of consistency between the two approaches.

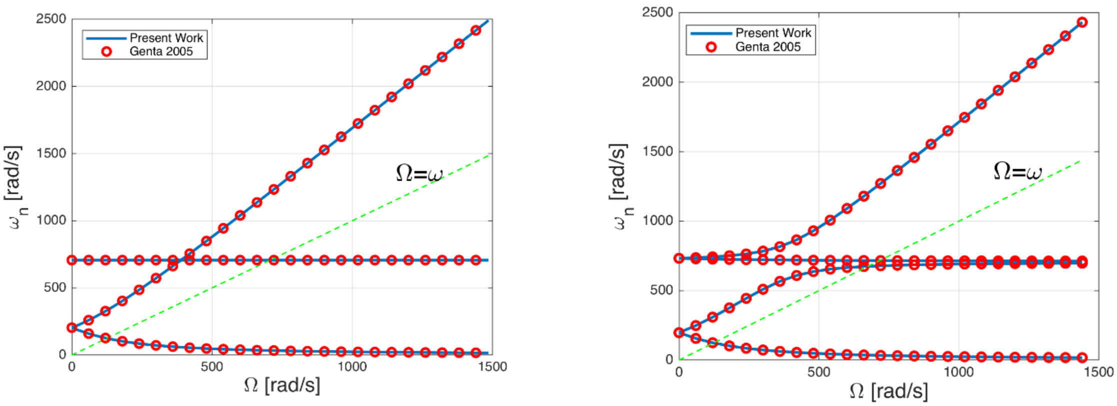

Fig 4. Comparison and validation of the results with Ref. (Genta, 2005).

3.1.1 Parametric Analysis

A shaft with nonlinear support by respective properties in **Table 1** is employed to evaluate the proposed formulation

Table 1. Parameter and value for study behavior of rotor-disc-bald in aerodynamic flow

Parameter	Ω (Hz)	V_∞(m/s)	α_b(degree)	C_b(cm)	ρ_∞(kg/m3)	R(m)	N_b	m_r(kg)	J_x,J_y
value	2e2	2e2	30	1	1.225	0.2	20	4	0.02

Parameter	J_P	C_x,C_y (N.m/s)	K_x,K_y (N/m)
value	0.0058	0.2	5e5

3.1.2 Effects of Rotating Speed on Instability of Rotor

Fig. 5. presents the dynamic response of the rotor system. Analysis of the rotor center displacement reveals that the linear configuration becomes dynamically unstable near a rotational speed of approximately Ω=1200 Hz.

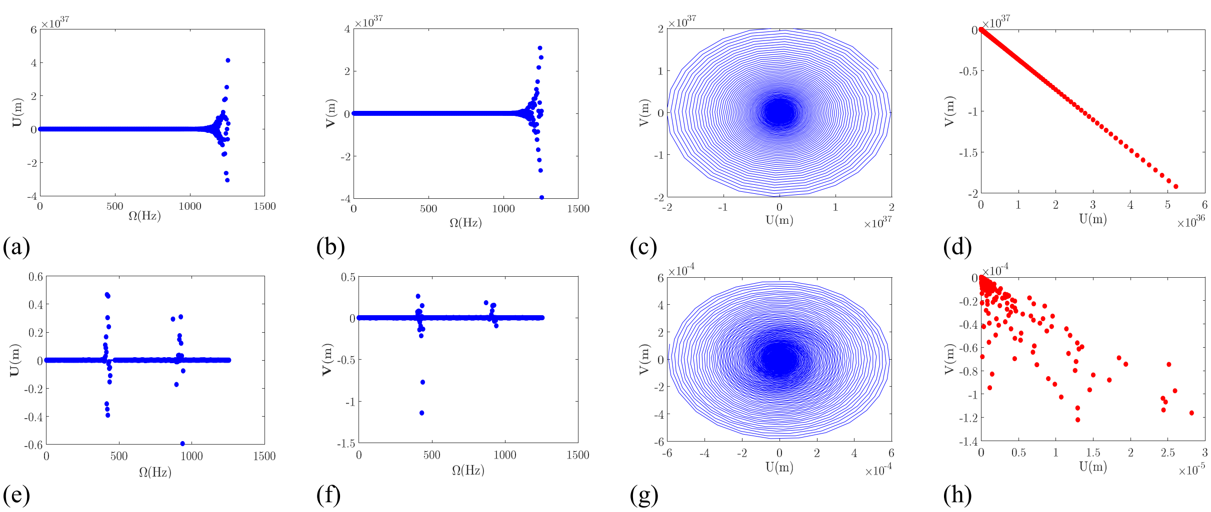

Fig. 5. The unstability behavior of a rotor turbine. a,b)biforcation diagram of linear rotor c,d) orbit and poincare map of linear rotor at **Ω** = 1200 [Hz], e,f)biforcation diagram of linear rotor g,h) orbit and poincare map of nonlinear rotor at **Ω** = 400 [Hz].

In contrast, the system with nonlinear supports exhibits instability near Ω=400 Hz, as evidenced by the increasing vibration amplitudes over time, particularly highlighted in **Fig. 5c** and **Fig. 5g**, which correspond to unstable rotational speeds. The bifurcation diagram displays a spread of discrete points, indicative of multi-periodic behavior—a dynamic state characterized by the presence of multiple incommensurate frequency components, commonly arising from the excitation introduced by nonlinear support elements. This interpretation is supported by the orbit plots and Poincaré maps shown in **Fig. 5c**, **Fig. 5g**, **Fig. 5d** and **Fig. 5h** at Ω=1200 Hz and Ω=400 Hz, respectively. The density and distribution of the points in the Poincaré sections reflect the number of vibration periods, thereby confirming the multi-periodic nature of the rotor's response under these conditions.

3.1.3 Effects of Aerodynamic Force Parameters on Instability of Rotor

In this section, the response of the rotor is illustrated and the unstable parameter is achieved by plotting various time responses of the rotor turbine. Thus, the stable and unstable responses corresponding to specific parameter are represented here.

3.2 Aerodynamic Speed

The effect of aerodynamic velocity on the system's stability margins is illustrated in **Fig 6** and **Fig. 7**. A comparative analysis of these results reveals the impact of airflow conditions on the onset and progression of dynamic instability. it is visible that at V_∞=35 and V_∞=32 m/s, the linear and nonlinear rotor become unstable, respectively. It is worth to mention that according to **Fig. 7**, the nonlinear shaft becomes unstable at a lower aerodynamic speed in comparison with linear one. Additionally, the unstable behavior is shown thorough orbit and Poincare map according to **Figs. 7c, 7g** and **Figs. 7d, 7h**.

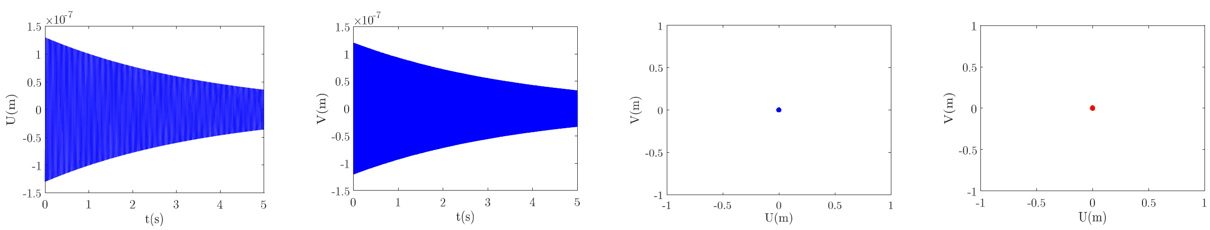

(a) (b) (c) (d)

Fig. 6. The behavior of a stable rotor turbine. a,b) Time response of linear/nonlinear rotor at V_∞<35 and 32 m/s c,d) orbit and poincare map of linear rotor at stable response.

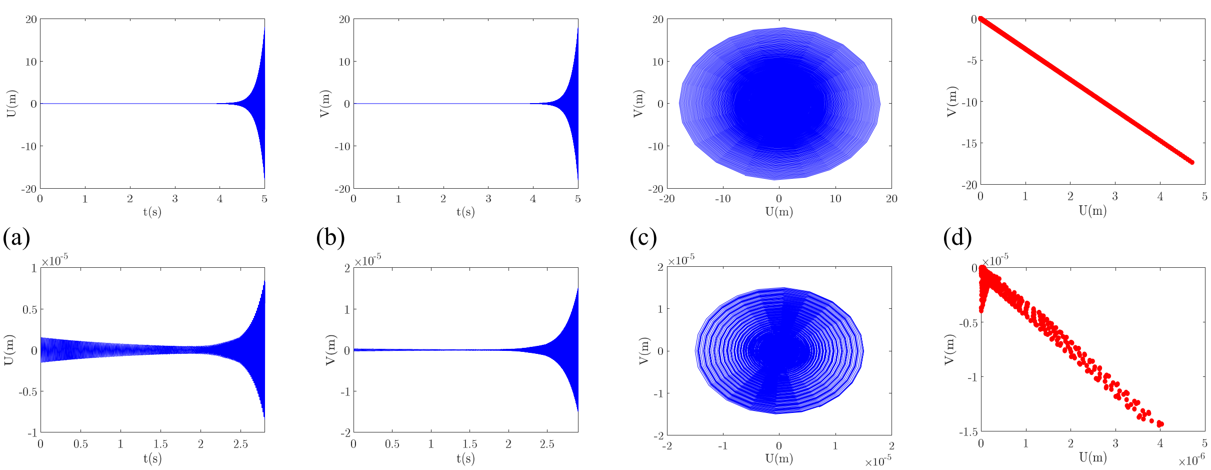

(a) (b) (c) (d)

(e) (f) (g) (h)

Fig. 7. The behavior of an unstable rotor turbine. a,b) Time response of linear rotor at V_∞=35 m/s c,d) orbit and poincare map of linear rotor at unstable response, e,f) Time response of nonlinear rotor at V_∞=32 m/s c,d) orbit and poincare map of nonlinear rotor at unstable response.

3.3 AOA

In this section, the influences of angle of attack on rotor response is taken into account for linear and nonlinear rotors through **Fig. 8** and **Fig. 9**. The amplitude and position are illustrated for linear and nonlinear rotors at α=26° and α=24° respectively, in **Fig. 9**. This result also illustrates the occurrence of spiral vibration, characteristic of unstable rotor trajectories under specific operating conditions. By a comparison between **Fig. 8** and **Fig. 9**, it is visible that at α=26° and α=24° the linear and nonlinear rotor become unstable, respectively.

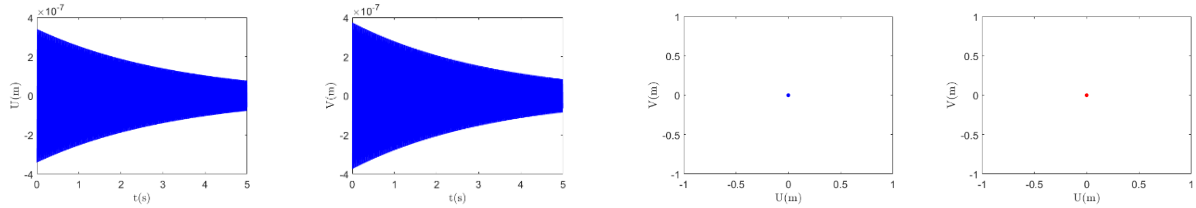

(a) (b) (c) (d)

Fig. 8. The behavior of a stable rotor turbine. a,b) Time response of linear/nonlinear rotor at α<26° and 24° c,d) orbit and poincare map of linear rotor at stable response.

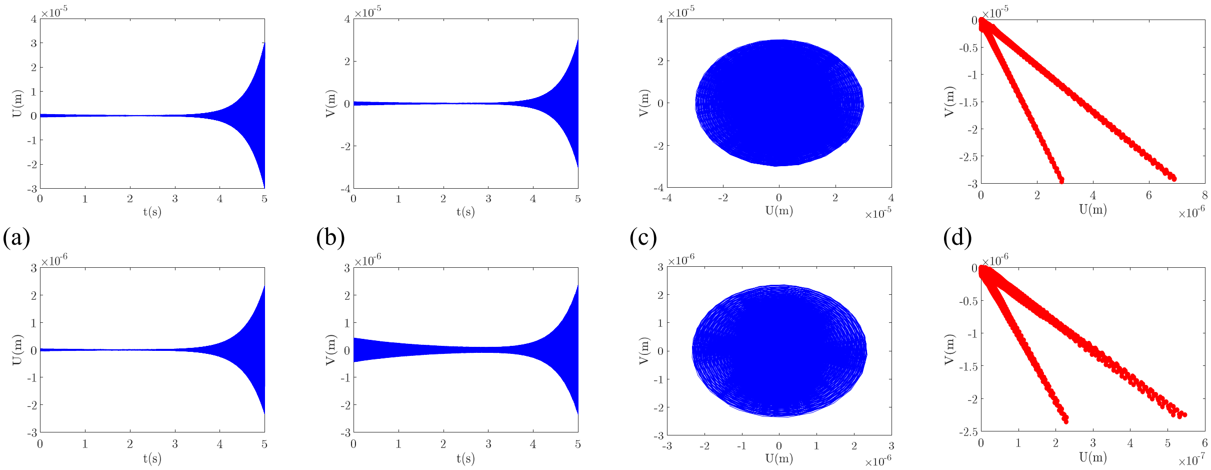

(a) (b) (c) (d)

(e) (f) (g) (h)

Fig. 9. The behavior of an unstable rotor turbine. a,b) Time response of linear rotor at α=26° c,d) orbit and poincare map of linear rotor at unstable response, e,f) Time response of nonlinear rotor at α=24° c,d) orbit and poincare map of nonlinear rotor at unstable response.

3.4 Density

Fig 10 and 11 further depict the rotor's dynamic response as a function of the density parameter, highlighting its influence on system behavior. By comparison between Fig. 10 and Fig. 11, it is visible that at ρ=1000 kg/m^3, the rotor become unstable. As can be seen, the density is an important parameter, which is capable of making a system unstable where interestingly, its effect on both linear and nonlinear rotors is similar to each other. Due to this similarity, only the nonlinear rotor response affected by density parameter is illustrated in Figs. 10 and 11.

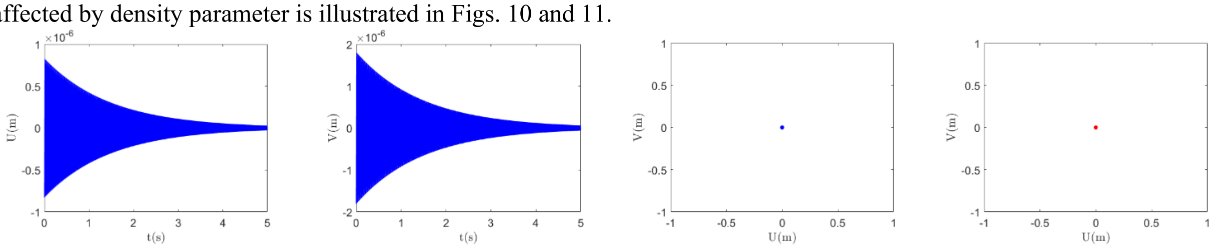

(a) (b) (c) (d)

Fig. 10: The behavior of a stable rotor turbine. a,b) Time response of linear/nonlinear rotor at ρ > 1000 kg/m^3 c,d) orbit and poincare map of linear rotor at stable response.

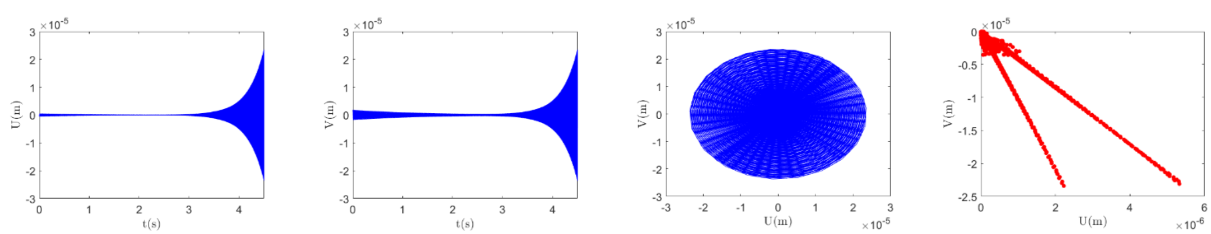

(a) (b) (c) (d)

Fig. 11. The behavior of an unstable rotor turbine. a,b) Time response of nonlinear rotor at ρ=1000 kg/m^3 c,d) orbit and poincare map of nonlinear rotor at unstable response.

3.4.1 Effects of Disk Radius on Instability of Rotor

The stability characteristics of both linear and nonlinear rotor systems are assessed through stability chart generated for varying disk radii and the unstable response is obtained at R = 19 cm and R = 18 cm for linear and nonlinear ones, respectively, according to **Fig. 12** and **Fig. 13**. By comparison between **Fig. 12** and **Fig. 13**, it is visible that at α=26° and α=24°, the linear and nonlinear rotor become unstable, respectively.

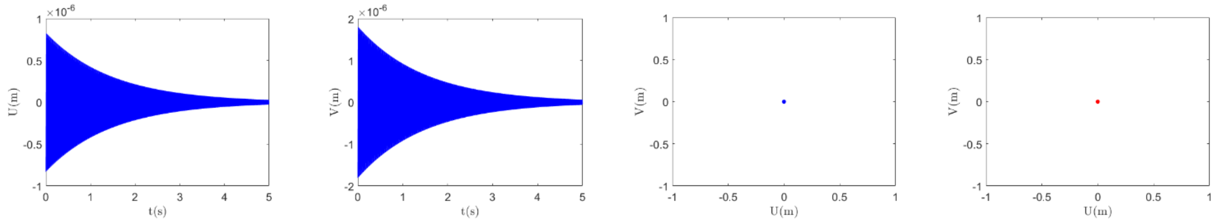

(a) (b) (c) (d)

Fig. 12. The behavior of a stable rotor turbine. a,b) Time response of linear/nonlinear rotor at R < 19 and 18 cm c,d) orbit and poincare map of linear rotor at stable response.

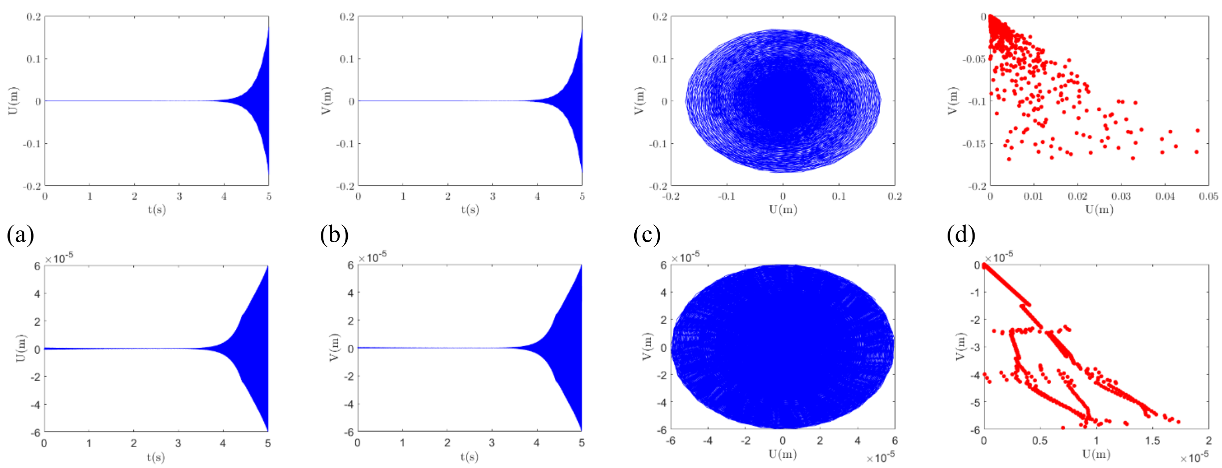

(a) (b) (c) (d)

(e) (f) (g) (h)

Fig. 13. The behavior of an unstable rotor turbine. a,b) Time response of linear rotor at R = 19 cm c,d) orbit and poincare map of linear rotor at unstable response, e,f) Time response of nonlinear rotor at R = 18 cm c,d) orbit and poincare map of nonlinear rotor at unstable response.

3.4.2 Effects of Support parameters on Instability of Rotor

The effect of support characteristics, namely stiffness and damping, on dynamic behavior of a rotor turbine are presented in **Fig. 14** and **Fig. 15**. This analysis offers valuable design insights for selecting appropriate rotor parameters to ensure stable operation and mitigate the risk of failure.

To get deep insights into the support parameters, **Fig. 14** and **Fig. 15** are illustrated for the stable and unstable rotors. According to **Fig. 14** and **Fig. 15**, The vibration amplitudes are significantly influenced by the support parameters, and instability arises within specific ranges of these parameters depending on the system's operating conditions in $K_x = K_y$ = 5e5 N/m and C_x = C_y = 0.2 N.m/s. Therefore, adjusting the support characteristics—specifically the levels of damping and stiffness—can be an effective strategy for achieving targeted dynamic behavior. In particular, increasing both stiffness and damping tends to suppress vibration amplitudes and enhance the overall stability of the rotor system.

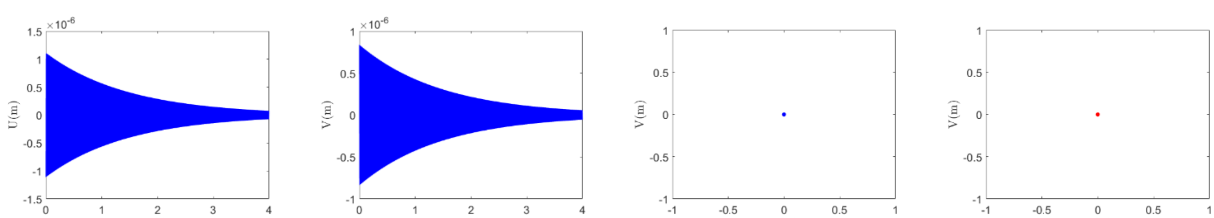

(a) (b) (c) (d)

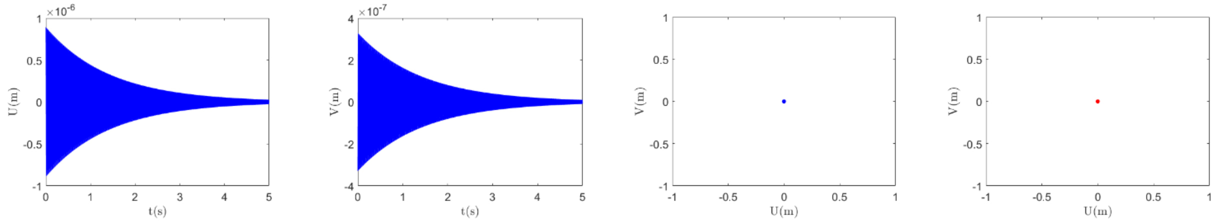

(e) (f) (g) (h)

Fig. 14. The behavior of a stable rotor turbine. a,b) Time response of linear rotor at K> 5e5 N/m c,d) orbit and poincare map of linear rotor at stable response, e,f) Time response of nonlinear rotor at C >0.2N.m/s c,d) orbit and poincare map of nonlinear rotor at stable response.

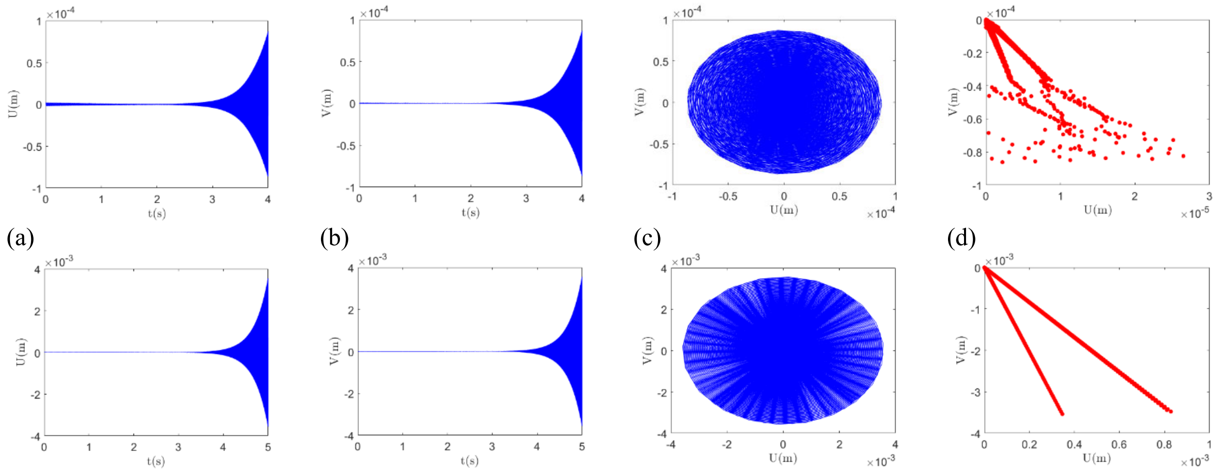

(e) (f) (g) (h)

Fig. 15. The behavior of an unstable rotor turbine. a,b) Time response of linear rotor at K= 5e5 N/m c,d) orbit and poincare map of linear rotor at unstable response, e,f) Time response of nonlinear rotor at C = 0.2N.m/s c,d) orbit and poincare map of nonlinear rotor at unstable response.

4. Conclusion

The present study examines the impact of nonlinear support properties on the aeroelastic stability of multi-stage turbine rotors subjected to aerodynamic excitation. By incorporating nonlinear stiffness and damping elements into a comprehensive dynamic model and solving the coupled aeroelastic equations via the Runge-Kutta method, the study captures key nonlinear phenomena including bifurcations and multi-periodic responses. The results demonstrate that:

– Nonlinear support elements significantly affect critical speeds and stability margins, especially under low to moderate aerodynamic speeds.
– Aerodynamic parameters such as flow velocity, angle of attack, and fluid density strongly influence rotor stability, often triggering instability earlier in nonlinear systems than in linear ones.
– Disk radius and support tuning (stiffness and damping) are shown to be critical design levers in managing instability risks.

Overall, the developed modeling framework and findings contribute to a deeper understanding of complex rotor–support–aerodynamics interactions, enabling more reliable and optimized design of turbine systems operating under realistic dynamic conditions.

References

Adamczyk, J., & Goldstein, M. (1978). Unsteady flow in a supersonic cascade with subsonic leading-edge locus. *AIAA journal*, *16*(12), 1248-1254.

Bornassi, S., Navazi, H., & Haddadpour, H. (2020). Coupled bending-torsion flutter investigation of MRE tapered sandwich blades in a turbomachinery cascade. *Thin-Walled Structures*, *152*, 106765.

Directorate, P. (2000). High Cycle Fatigue (HCF) Program 1999 Annual Report. *Paper No. AFRL-PR-WP-TR-2000-2004*.

Dowell, E. H., & Dowell, E. H. (2015). Nonlinear aeroelasticity. *A Modern Course in Aeroelasticity: Fifth Revised and Enlarged Edition*, 487-529.

Genta, G. (2005). *Dynamics of rotating systems*. Springer Science & Business Media.

Kim, D., Lee, A. S., & Choi, B. S. (2014). Evaluation of foil bearing performance and nonlinear rotordynamics of 120 kW oil-free gas turbine generator. *Journal of Engineering for Gas Turbines and Power*, *136*(3).

Kosmatka, J., & Mehmed, O. (1998). Experimental spin testing of integrally damped composite blades. 39th AIAA/ASME/ASCE/AHS/ASC Structures, Structural Dynamics, and Materials Conference and Exhibit,

Kosmatka, J. B., Lapid, A. J., & Mehmed, O. (1995). Passive vibration reduction of advanced composite pretwisted plates using integral damping materials. Smart Structures and Materials 1995: Passive Damping,

Li, Z., Li, Z., Li, J., & Feng, Z. (2022). Static and Rotordynamic Characteristics for Two Types of Novel Hole-Pattern Seals Operating in Supercritical CO2 Turbomachinery. *Journal of Engineering for Gas Turbines and Power*, *144*(7), 071006.

Liu, W., Kim, D., & Feng, K. (2018). Effect of axial force on rotordynamics of a rigid rotor supported by foil bearings. Turbo Expo: Power for Land, Sea, and Air,

Moore, J. J., Ransom, D. L., & Viana, F. (2011). Rotordynamic force prediction of centrifugal compressor impellers using computational fluid dynamics. *Journal of Engineering for Gas Turbines and Power*, *133*(4).

Palanca, C., Engeda, A., & Cave, M. (2020). Investigation of Rotordynamic Coefficients of Gas Labyrinth Seals Using a Steady State CFD Approach. *Turbo Expo: Power for Land, Sea, and Air*, *84225*, V10BT29A007.

Seeley, C. E., Wakelam, C., Zhang, X., Hofer, D., & Ren, W.-M. (2017). Investigations of flutter and aerodynamic damping of a turbine blade: Experimental characterization. *Journal of Turbomachinery*, *139*(8).

Smith, S. N. (1972). Discrete frequency sound generation in axial flow turbomachines.

Subramanian, S., Sekhar, A., & Prasad, B. (2016). Rotordynamic characteristics of rotating labyrinth gas turbine seal with centrifugal growth. *Tribology International*, *97*, 349-359.

Wang, B., Sun, Y., & Ding, Q. (2020). Free fluid-structure interaction method for accurate nonlinear dynamic characteristics of the plain gas journal bearings. *Journal of Vibration Engineering & Technologies*, *8*(1), 149-161.

Whitehead, D. (1962). Force and moment coefficients for vibrating airfoils in cascade [Internet]. In: London: Her Majesty's Stationery Office.

Żywica, G., Breńkacz, Ł., & Bagiński, P. (2018). Interactions in the rotor-bearings-support structure system of the multi-stage ORC microturbine. *Journal of Vibration Engineering & Technologies*, *6*(5), 369-377.